Food & Function

ROYAL SOCIETY OF CHEMISTRY

PAPER

View Article Online
View Journal | View Issue

Cite this: *Food Funct.*, 2026, **17**, 991

Lactobacillus fermentum remodeled the lung microbiota by crosstalk with the gut and lungs and regulated the PI3K–AKT pathway to alleviate acute lung injury

Jiali Ni,†[a] Jian Shen,†[b] Fengjiao Wang,[a] Yechen Wu,[c] Bo Qiu,[a] Ziyuan Zhou,[a] Qianhan Xie,[a] Shengjie Li,[a] Qiangqiang Xiang,[a] Tinglei Song,[a] Yuxi Zhao,[a] Yanfei Chen*[a] and Lanjuan Li *[a]

Acute lung injury (ALI) is a syndrome of acute inflammatory lung injury triggered by diverse etiological factors, which can lead to atelectasis, prolonged hypoxemia, severe respiratory distress, and high mortality. There is increasing evidence that the gut microbiota is involved in regulating pulmonary immunity, and the gut–lung axis plays a critical role in pulmonary diseases. The primary objective of this study was to investigate the effect of *Lactobacillus fermentum* on lipopolysaccharide (LPS)-induced ALI. After the establishment of an LPS-induced ALI model and gavage with *L. fermentum*, pulmonary edema and inflammatory cell infiltration in mice were significantly reduced. In addition, *L. fermentum* regulated the gut microecology, restored the gut barrier, remodeled the lung microecology and increased the abundance of Lactobacillaceae through gut–lung cross-talk. Multi-omics results suggested that *L. fermentum* intervention regulated sphingolipid metabolism and downregulated the PI3K–AKT pathway. Moreover, intervention of lung organoids with the cell-free supernatant (CFS) of *L. fermentum* significantly reduced LPS-induced autoinflammatory responses and confirmed the down-regulation of the PI3K–AKT signaling pathway. In conclusion, *L. fermentum* alleviates LPS-induced lung injury by regulating the PI3K–AKT signaling pathway *via* the gut–lung axis, offering a potential therapeutic approach for ALI.

Received 27th October 2025,
Accepted 27th November 2025

DOI: 10.1039/d5fo04619j

rsc.li/food-function

Introduction

Acute lung injury (ALI) is a rapidly progressing lung condition characterized by diffuse inflammation and injury, which can be triggered by various pathogenic factors.[1] ALI may lead to atelectasis, long-term hypoxemia, severe respiratory distress, and even acute respiratory distress syndrome (ARDS).[1,2] However, treatment for ALI is limited, and the mortality rate is as high as 40%.[3] The primary approach of ALI treatment involves lung-protective ventilation and fluid management, with the addition of therapies such as glucocorticoids, inhaled pulmonary vasodilators, neuromuscular blockade, or extracorporeal membrane oxygenation as needed.[4]

The gut–lung axis serves as a critical pathway through which gut microbiota and their metabolites influence lung immunity.[5] The development of pulmonary diseases has been consistently linked to gut dysbiosis, characterized by a decline in *Bifidobacterium*, *Blautia*, *Faecalibacterium prausnitzii*, *Lactobacillus*, and *Akkermansia*, and an increase in *Proteobacteria*, *Escherichia-Shigella*, *Enterococcus*, *Parasutterella*, and *Alloprevotella*, as observed in community-acquired pneumonia, acute pancreatitis-induced ALI/ARDS, COVID-19, and ALI mouse models.[6–12]

Targeting the gut microbiota presents a viable strategy for ameliorating lung injury. Fecal microbiota transplantation can rapidly restore microbial communities and mitigate lung cell apoptosis by improving gut pathology and systemic immunity.[13,14] Similarly, direct probiotic supplementation demonstrated efficacy. For instance, *Akkermansia muciniphila* exerted anti-inflammatory effects *via* its metabolite butyrate, inhibiting the TLR2/MyD88/NF-κB pathway.[15] Clinical trials

[a]*State Key Laboratory for Diagnosis and Treatment of Infectious Diseases, National Clinical Research Center for Infectious Diseases, China-Singapore Belt and Road Joint Laboratory on Infection Research and Drug Development, National Medical Center for Infectious Diseases, Collaborative Innovation Center for Diagnosis and Treatment of Infectious Diseases, The First Affiliated Hospital, Zhejiang University School of Medicine, Hangzhou City 310003, China. E-mail: chenyf_zju@zju.edu.cn, ljli@zju.edu.cn*

[b]*Cancer Center, Department of Gastroenterology, Zhejiang Provincial People's Hospital (Affiliated People's Hospital), Hangzhou Medical College, Hangzhou, Zhejiang, China*

[c]*Shandong First Medical University, Jinan Microecological Biomedicine Shandong Laboratory, Jinan City 250022, China*

†These authors contributed equally to this work.

further supported this approach; supplementation with *Lactobacillus fermentum* alleviated respiratory and gastrointestinal symptoms in athletes, and a probiotic formulation containing *Lactiplantibacillus* and *Pediococcus* improved outcomes in COVID-19 patients.[16,17] Collectively, these findings underscored that modulating the gut microbiota, either directly or indirectly, interacted with the host immune system to confer protection against lung injury.

Limosilactobacillus fermentum (*Lactobacillus fermentum*), a widely used probiotic strain isolated from fermented grain-based foods, exhibited notable acid and bile tolerance—a key probiotic property that supports survival under harsh gastrointestinal conditions and is also valuable for food industry applications.[18,19] Its probiotic efficacy has been attributed to a variety of mechanisms, including the ability to form intestinal biofilms, which inhibit pathogen colonization, modulate immune responses, and reduce the production of pro-inflammatory factors.[18,20,21] These properties supported its protective role in various disease models. In a mouse influenza model, the abundance of *Lactobacillus* was consistently reduced in the oropharynx, nasopharynx, lungs, and gut, highlighting the potential of *Lactobacillus* as a therapeutic target for pulmonary infections.[22]

Lactobacillus can secrete acids, bacteriocins and other by-products, which can neutralize the infections caused by pathogens and regulate the host's inflammatory and immune responses.[23] A study on the anti-inflammatory activity of probiotic metabolites found that the cell-free supernatant of various *Lactobacillus* strains (*Lactobacillus acidophilus*, *Lactobacillus casei*, *Lactobacillus reuteri*, *etc.*) exhibited specific anti-inflammatory activity, regulating the production of IL-1β, IL-6, TNF-α, and IL-10.[24] The CFS of *L. fermentum* also has certain anti-inflammatory and anti-oxidant stress effects.[25] The research on cellular anti-aging has found that the CFS of *L. fermentum* significantly reduced key aging markers, including the expression of p53/p21WAF1 and SA-β-Gal, while inhibiting p38MAPK, NF-κB, oxidative stress (iNOS, COX-2 and ROS) and DNA damage.[26] Considering the low pH properties of *L. fermentum*, we conducted an *in vitro* intervention experiment using the CFS of the lactic acid bacteria.

This study focused on the role of *Lactobacillus fermentum* in regulating the immune function of the gut–lung axis. Leveraging comprehensive multi-omics analysis (16S sequencing, transcriptomics, and metabolomics), this study evaluated the effect of *L. fermentum* on LPS-induced ALI and sought to uncover its underlying mechanism.

Results

L. fermentum attenuates inflammation and preserves the pulmonary barrier function

A stable ALI model was successfully established *via* a single administration of LPSs (Fig. 1A). As shown in Fig. 1B and C, while *L. fermentum* gavage did not adversely affect body weight over 21 days ($p > 0.05$), the LF group exhibited a slower rate of weight loss after LPS induction compared to the LPS group ($p < 0.05$). Compared to the LPS group, the LF group exhibited a lower lung W/D ratio (Fig. 1D, $p < 0.01$), indicating less severe pulmonary edema. The total protein concentration, cell number, and the LDH activity in the LF group were significantly improved (LF *vs.* LPS, $p < 0.05$, $p < 0.01$ and $p < 0.001$, respectively), suggesting that the alveolar barrier was repaired after *L. fermentum* intervention. The lung injury score and H&E staining (Fig. 1H and I) showed that mice in the LPS group had diffuse inflammatory cell infiltration in the alveoli and interstitium, thickening of the alveolar walls and interstitium, and severe damage or disappearance of normal lung structure. Compared with the LPS group, the LF group demonstrated markedly ameliorated lung histopathology, characterized by lower injury scores, thinner alveolar walls, and reduced inflammatory cell infiltration. These results indicated that *L. fermentum* can reduce inflammatory cell infiltration and pulmonary edema, and protect the lung barrier function.

The study found that *L. fermentum* significantly reduced the acute inflammatory response caused by LPS. In BALF, the levels of IL-1β and IL-6 in the LF group were significantly decreased (Fig. 1J and K, LF *vs.* LPS, $p < 0.01$ and $p < 0.05$). In serum, the levels of IL-1β, IL-6, TNF-α and MCP1 in the LF group were significantly lower than those in the LPS group (Fig. 1L–O, LF *vs.* LPS, $p < 0.01$, $p < 0.05$, $p < 0.05$, and $p < 0.001$, respectively). Furthermore, immunohistochemical analysis of F4/80 and MPO (Fig. 1P and Q) revealed that the *L. fermentum* intervention significantly improved the aggregation of macrophages and neutrophils in the lungs induced by LPS.

L. fermentum improves the gut barrier function and regulates gut metabolism

Serum LBP concentrations were measured to reflect gut permeability and serve as a marker for the translocation of gut microorganisms and of systemic LPS exposure.[27] Compared with the NC group, the LBP level of serum in the LPS group was significantly increased (Fig. 2A, LPS *vs.* NC, $p < 0.001$), and it was significantly decreased in the LF group (LF *vs.* LPS, $p < 0.01$). We measured the mRNA expression levels of several typical gut barrier factors, like zonula occludens protein 1 (ZO-1), mucin 2 (MUC-2), and Occludin (Fig. 2B). At the mRNA level (Fig. 2B), the relative mRNA expression of MUC-2, Occludin, and ZO-1 in the colonic tissue was significantly downregulated in the LPS group compared to the NC group (LPS *vs.* NC, $p < 0.001$, $p < 0.001$ and $p < 0.01$, respectively). *L. fermentum* gavage effectively reversed this trend, upregulating their expression compared to the LPS group (LF *vs.* LPS, $p < 0.001$, $p < 0.001$ and $p < 0.05$, respectively). Immunofluorescence was used to detect the protein expression of ZO-1, MUC-2 and Occludin (Fig. 2C). We found that the tight junction structure and mucus layer thickness of the gut mucosa were restored after *L. fermentum* intervention.

LPS induction significantly altered the gut metabolism (SI Fig. S1A and B and Fig. 2D). Compared to the LF group with the LPS group, lipid metabolites were elevated in the LPS group, including multiple sphingolipids (SL 14:3;O/16:4,

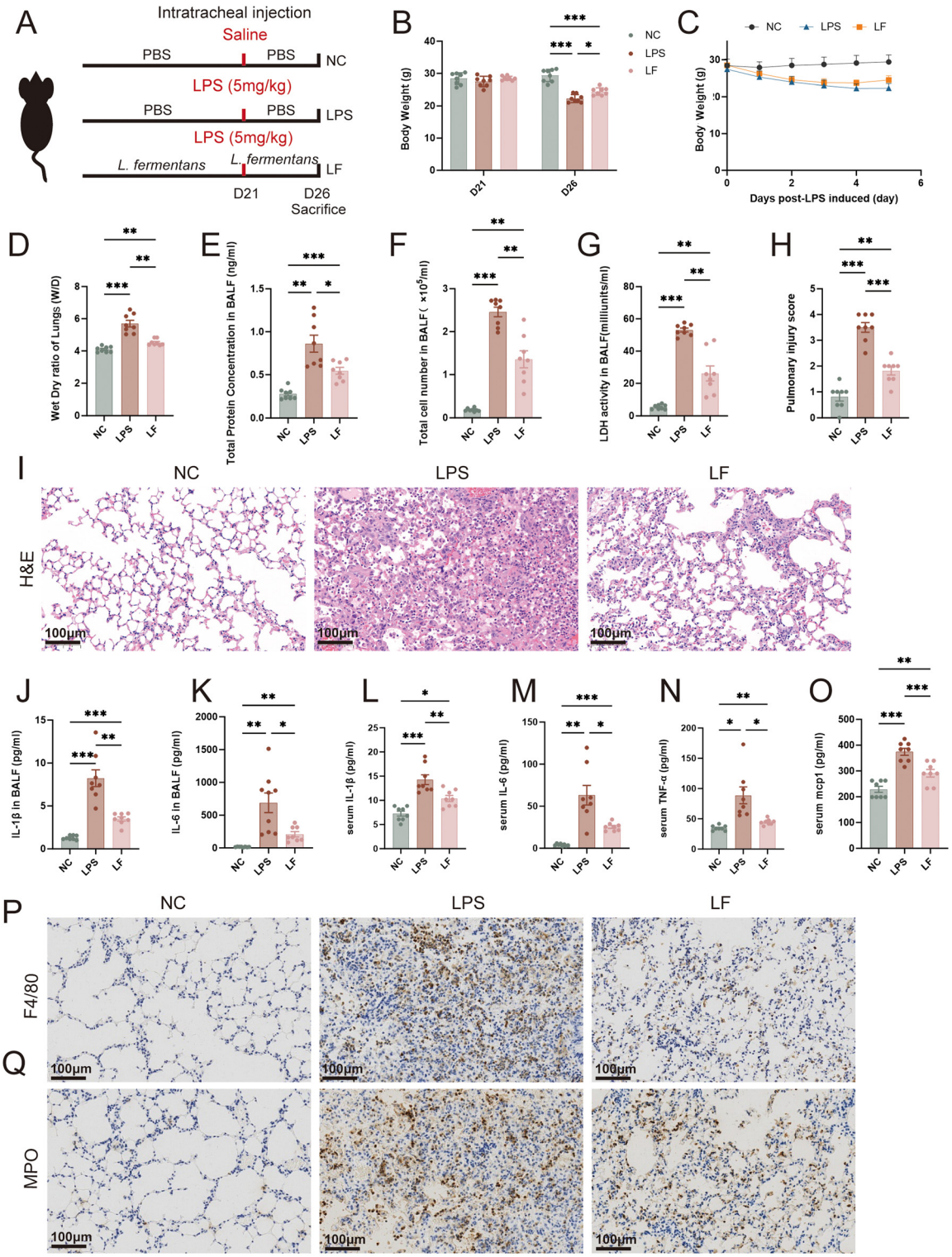

Fig. 1 (A) LPS was used to establish a stable model of acute lung injury. (B) Bar graph of body weight after 21 days of *L. fermentum* gavage and after 5 days of LPS induction. (C) Curves of body weight changes after LPS induction. (D) Wet dry ratio (W/D) of the lungs. (E and F) Total protein concentration and total cell number in BALF. (G) LDH activity. (H) Pulmonary injury score. (I) H&E staining in the lung tissue. (J and K) The levels of IL-1β and IL-6 in BALF. (L–O) The levels of IL-1β, IL-6, TNF-α, and MCP1 in serum. (P and Q) Immunohistochemical staining of F4/80 and MPO in lung tissue. Data are presented as the mean ± standard error of the mean (mean ± SEM); $*p < 0.05$, $**p < 0.01$ and $***p < 0.001$.

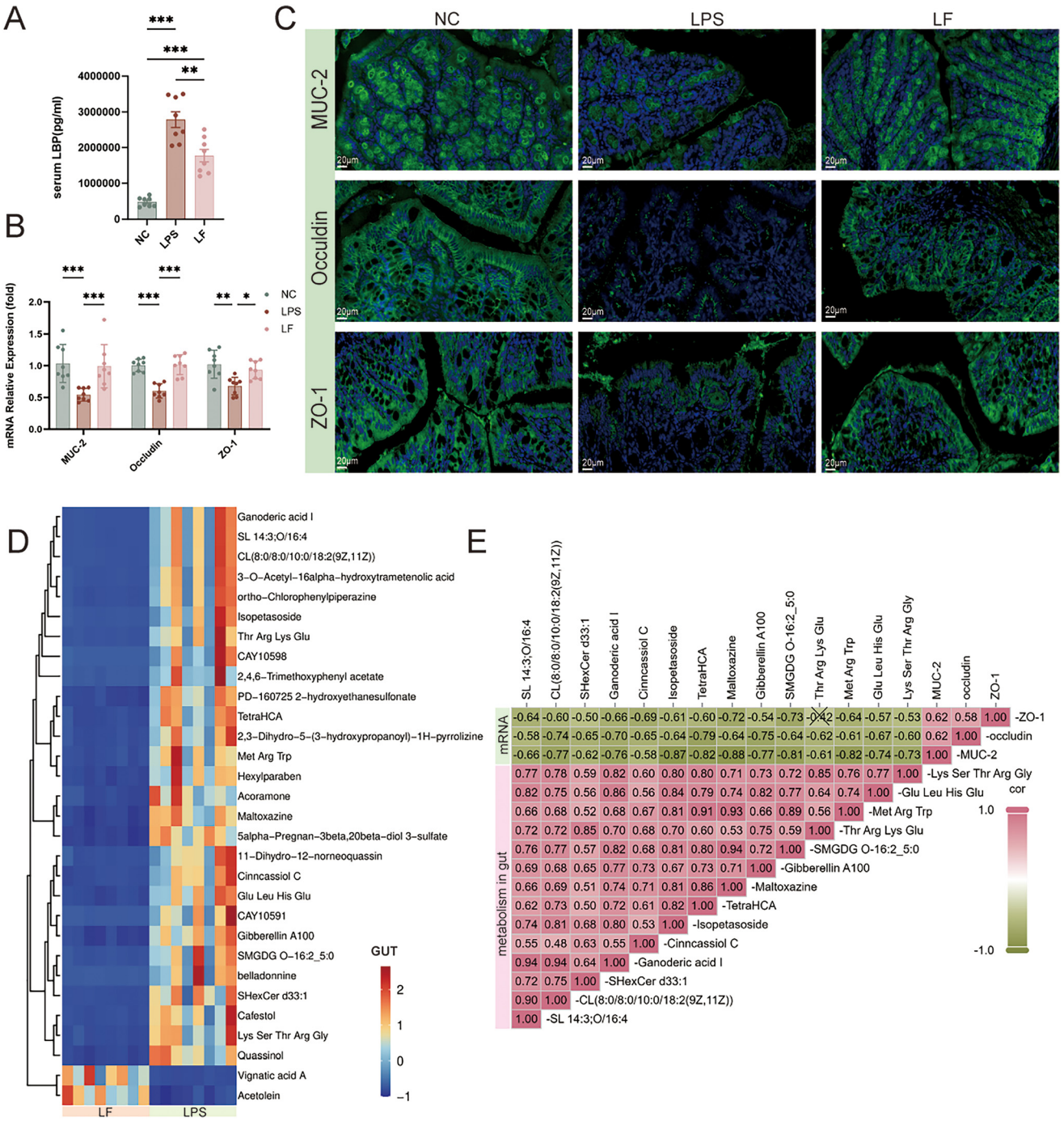

Fig. 2 (A) Serum LBP level. (B) Relative mRNA expression levels of MUC-2, Occludin, and ZO-1; GAPDH was used as the internal reference. (C) Immunofluorescence staining of MUC-2, Occludin, and ZO-1 expression in colonic tissues. (D) Heat map of the top 30 differential metabolites in the gut. (E) A correlation analysis between the key metabolites and the expression of mRNA related to the gut barrier was conducted using the Spearman analysis; the symbol "×" indicates that $p > 0.05$. Data are presented as the mean ± standard error of the mean (mean ± SEM); $^{*}p < 0.05$, $^{**}p < 0.01$ and $^{***}p < 0.001$.

SHexCer d33:1) and cardiolipin (CL(8:0/8:0/10:0/18:2(9*Z*,11*Z*))). The changes of the lipid composition and function of the cell membrane suggested damage to the gut cell barrier. The increased levels of ganoderic acid, cinncassiol C, isopetasoside and TetraHCA reflect the compensatory increase of gut injury in the LPS group. The elevated levels of Maltoxazine, Gibberellin A100 and SMGDG O-16:2_5:0 in the gut indicate an imbalance of the intestinal flora, which is caused by an increase in the number of harmful bacteria. Increased peptides, such as Thr–Arg–Lys–Glu, also suggest gut metabolic dis-

orders. LPS-induced inflammation leads to a shift in the gut metabolic environment to a pro-inflammatory and disordered state. The expression levels of these metabolites were negatively correlated with those of gut barrier-related genes (ZO-1, MUC-2 and Occludin) (Fig. 2E). After *L. fermentum* intervention, the gut barrier was repaired, gut inflammation was reduced and gut immune activation was balanced.

L. fermentum restored the gut microbiota in LPS-induced acute lung injury

The gut microbiota showed significant structural and abundance abnormalities. In terms of α-diversity, the Chao1 and Shannon indices were significantly decreased (Fig. 3A, LPS *vs.* NC, $p < 0.05$ and $p < 0.05$). The PCoA analysis of β-diversity also revealed abnormalities in the LPS group. After supplementing *L. fermentum* by gavage, the PCoA plot of β-diversity analysis showed that the gut species composition structure of the LF group changed to that of the NC group (Fig. 3B). As shown in Fig. 3C, the relative abundances of Lachnospiraceae, Prevotellaceae, Lactobacillaceae, Ruminococcaceae, and Enterobacteriaceae in the LF group were increased, compared to the LPS group. Linear discriminant analysis (LDA) was used to illustrate the biological differences in the gut microbiota (Fig. 3D and E). Compared with the NC group, LPS induced increased abundance of Rhodospirillales at the order level, Oscillospiraceae, Bacteroidaceae and Tannerellaceae at the family level, and *Bacteroides* and *Parabacteroides* at the genus level. Compared with the NC group, the LF group increased the abundance of Oscillospiraceae at the family level, and *Prevotellaceae_NK3B31_group* at the genus level. Compared with the LPS group, the LF group increased the abundance of Firmicutes at the phylum level, Bacilli at the class level, Lactobacillales at the order level, Lactobacillaceae at the family level, and *Ligilactobacillus*, *Lachnospiraceae_NK4A136_group* and *Prevotellaceae_NK3B31_group* at the genus level.

L. fermentum reshaped the lung microecology and regulated lung metabolism

Pronounced compositional differences in the lung microbiota were observed, with the LF group significantly distinct from the other two groups in the Chao1 index in α-diversity and in PCoA analysis in β-diversity (Fig. 4A and B). These results indicate that the changes of the gut microbiota after *L. fermentum* supplementation affected the species structure and abundance of the pulmonary microbiota at the same time, and a new pulmonary microbial system was constructed. As shown in Fig. 4C, the abundance of Lactobacillaceae increased in the LF group, as shown in the column plots of species abundance. LEfSe analysis is shown in Fig. 4D and E (LDA > 3). Compared with the NC group, the LPS group increased the abundance of *Acidovorax* at the genus level and Blastocatellia at the class level. Compared with the LPS group, the LF group increased the abundance of Enterobacteriaceae and Pseudomonadaceae at the family level, Pseudomonadales and Lactobacillales at the order level, *Latilactobacillus* and *Pseudomonas* at the genus level, *etc*. In addition, the abundances of *f_Bacteroidaceae*, *g_Bacteroides*, and f_Tannerellaceae were all increased in the lungs and gut of the LPS group (LPS *vs.* LF).

Similarly, LPS and *L. fermentum* also caused changes in the levels of metabolites in the lungs (SI Fig. S1C and D and Fig. 4F). Compared with the LF group, the down-regulated lung metabolites in the LPS group were mainly sphingolipid signaling molecules involved in cell apoptosis and inflammation, including multiple sphingolipids, as shown by SHexCer14:3; 2O/12:1; O, SL17:0; O/15:0; O, SL17:0; O/16:0, SL17:0; O/15:0, SL18:0; O/16:0, SL16:0; O/14:0, SL17:0; O/14:0, Cer(d16:1/PGE2), Cer(d16:1/PGF2alpha), *etc*., whose depletion may impair lung barrier function and signal transduction (Fig. 4F). As an important chemotactic factor, leukotriene B4 may be related to the blocked recruitment or depletion of immune cells to the lungs. The decrease in amino acids and their derivatives, such as ornithine-CA and His–Ser–Lys–Lys, may reflect a decrease in the metabolic capacity of lung function. The significant up-regulation of 3-guanidinopropanoate, a product of oxidative stress, further suggested that LPS caused lung injury through oxidative stress.

L. fermentum modulates the lung transcriptome in LPS-induced lung injury

The transcriptome analysis of lungs showed that there was a significant separation between different groups in the principal component space, and the LPS group and the LF group had significant differences in gene expression (Fig. 5A). The Venn diagram showed that a total of 4888 genes were detected (Fig. 5B). Comparison of the LPS and LF groups revealed 485 up-regulated genes and 1139 down-regulated genes in the LPS group (Fig. 5C). These genes were annotated against the KEGG pathway database to identify significantly enriched pathways and 13 significant signaling pathways were identified. Among them, the disease-related pathways were the PI3K–AKT signaling pathway, the TGF-β signaling pathway, focal adhesion, the ECM–receptor interaction, complement and coagulation cascades, and phagosome and platelet activation (Fig. 5D). As shown in Fig. 4E, by mapping key genes through the PI3K–AKT signaling pathway, we detected the following key genes that were significantly expressed in the LPS group: *Tnc*, *Fn1*, *Fgfr1*, *Areg*, *Ntrk2*, *Thbs1*, *Cdkn1a*, *Myc*, and *Ngf*. Among them, the significantly up-regulated genes *Fn1*, *Thbs1*, *Areg*, *Ntrk2*, and *Ngf* activated the PI3K–AKT/NF-κB signaling pathway, promoting inflammatory factor infiltration and alveolar epithelial barrier damage. As shown in Fig. 5F–I, the mRNA relative expression of PI3K, AKT, iNOS, and NF-κB in the LPS group was significantly upregulated, and was significantly reduced in the LF group (LF *vs.* LPS, $p < 0.001$, $p < 0.01$, $p < 0.05$ and $p < 0.001$, respectively).

Fig. 5J shows that Lactobacillaceae were positively correlated with sphingolipids and f_Tannerellaceae were negatively correlated with sphingolipids. The PI3K–AKT pathway genes *Ntrk2* and *Myc* were significantly correlated with sphingolipids, lung microbiota, and inflammatory damage factors. These results indicated that *L. fermentum* intervention increased the abundance of Lactobacillaceae in the lungs through gut–lung axis crosstalk,

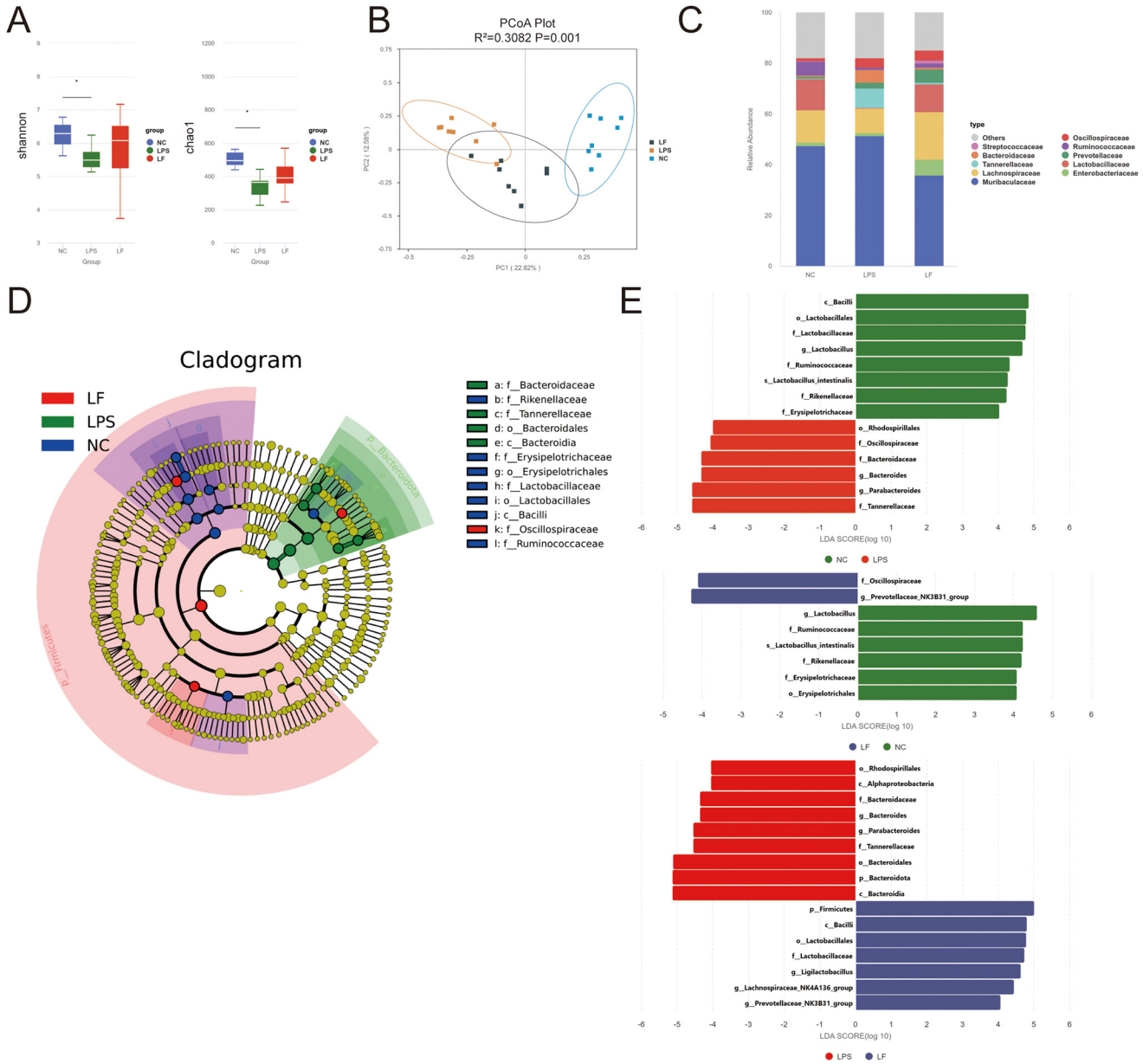

Fig. 3 (A) α-Diversity analysis using the Kruskal–Wallis test of the gut microbiota; the left portion indicates the Shannon index and the right portion indicates the Chao1 index. (B) PCoA based on the Bray–Curtis distance algorithm of β-diversity analysis of the gut microbiota. (C) Species abundance of the family level bar chart of the gut microbiota. (D and E) The LEfSe evolutionary branch diagrams and LDA value distribution bar chart of the NC group, the LF group and the LPS group of the gut microbiota (LDA > 4). Data are presented as the mean ± standard error of the mean (mean ± SEM); $*p < 0.05$, $**p < 0.01$ and $***p < 0.001$.

affected sphingolipid metabolism, regulated PI3K–AKT pathway genes, and ameliorated LPS-induced lung tissue cell injury.

CFS of *L. fermentum* protected the lung organoids from LPS injury

The *in vitro* experiments revealed that after LPS induction, the alveolar organoids underwent significant changes, with the levels of IL-6 and TNF-α secreted increasing significantly. After CFS intervention, the levels of IL-6 and TNF-α did indeed decrease (Fig. 6A and B, LPS-Ls *vs.* LPS, $p < 0.05$ and $p < 0.01$). The results indicated that the relative mRNA expression levels of genes related to alveolar epithelial organoids in the LPS group (PI3K, AKT, NF-κB and TNF-α) were significantly increased. After CFS intervention, the expression levels of these mRNAs decreased (Fig. 6C and D, LPS-Ls *vs.* LPS, $p < 0.01$, $p < 0.001$, $p < 0.05$ and $p < 0.01$, respectively). The CFS of *L. fermentum* improved the acute inflammatory response of the lung alveolar organoids induced by LPS.

In Fig. 6G, in the Ctrl group, the lung organoids showed intact organoid structures, presenting regular circular or ellip-

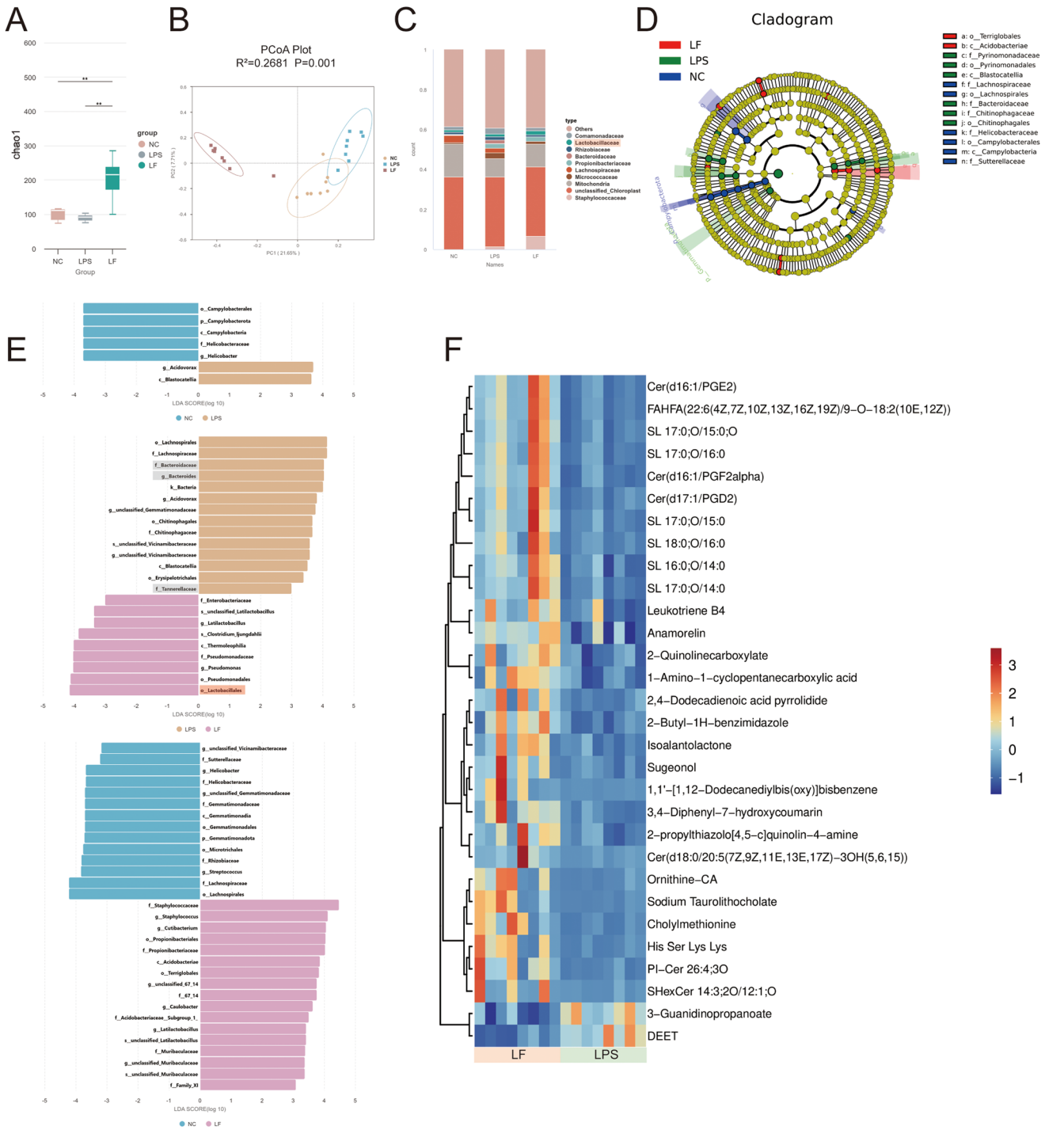

Fig. 4 (A) Chao1 index using the Kruskal–Wallis test of α-diversity analysis of the lung microbiota. (B) PCoA based on the Bray–Curtis distance algorithm of β-diversity analysis of the lung microbiota. (C) Species abundance of the family level bar chart of the lung microbiota. (D and E) The LDA value distribution bar chart of the NC group, the LF group and the LPS group of the lung microbiota (LDA > 3); the species marked in the gray boxes showed an increase in abundance in the LPS groups of lung and gut microbiota (LPS *vs.* LF), while the species marked in the pink boxes showed an increase in abundance in the LF groups of lung and gut microbiota (LPS *vs.* LF). (F) Heat map of the top 30 differential metabolites in the lungs. Data are presented as the mean ± standard error of the mean (mean ± SEM); $*p < 0.05$, $**p < 0.01$ and $***p < 0.001$.

tical cavities with smooth inner surfaces. The epithelial cells were arranged in a single layer closely and the cell nuclei had regular shapes and uniform sizes. In the LPS group, obvious changes such as cavity enlargement, thickening of the epithelial layer, disordered cell arrangement, nuclear shrinkage, and infiltration of inflammatory cells were observed. These typical pathological features indicated that LPS-induced injury caused significant inflammatory tissue damage. In Fig. 6H,

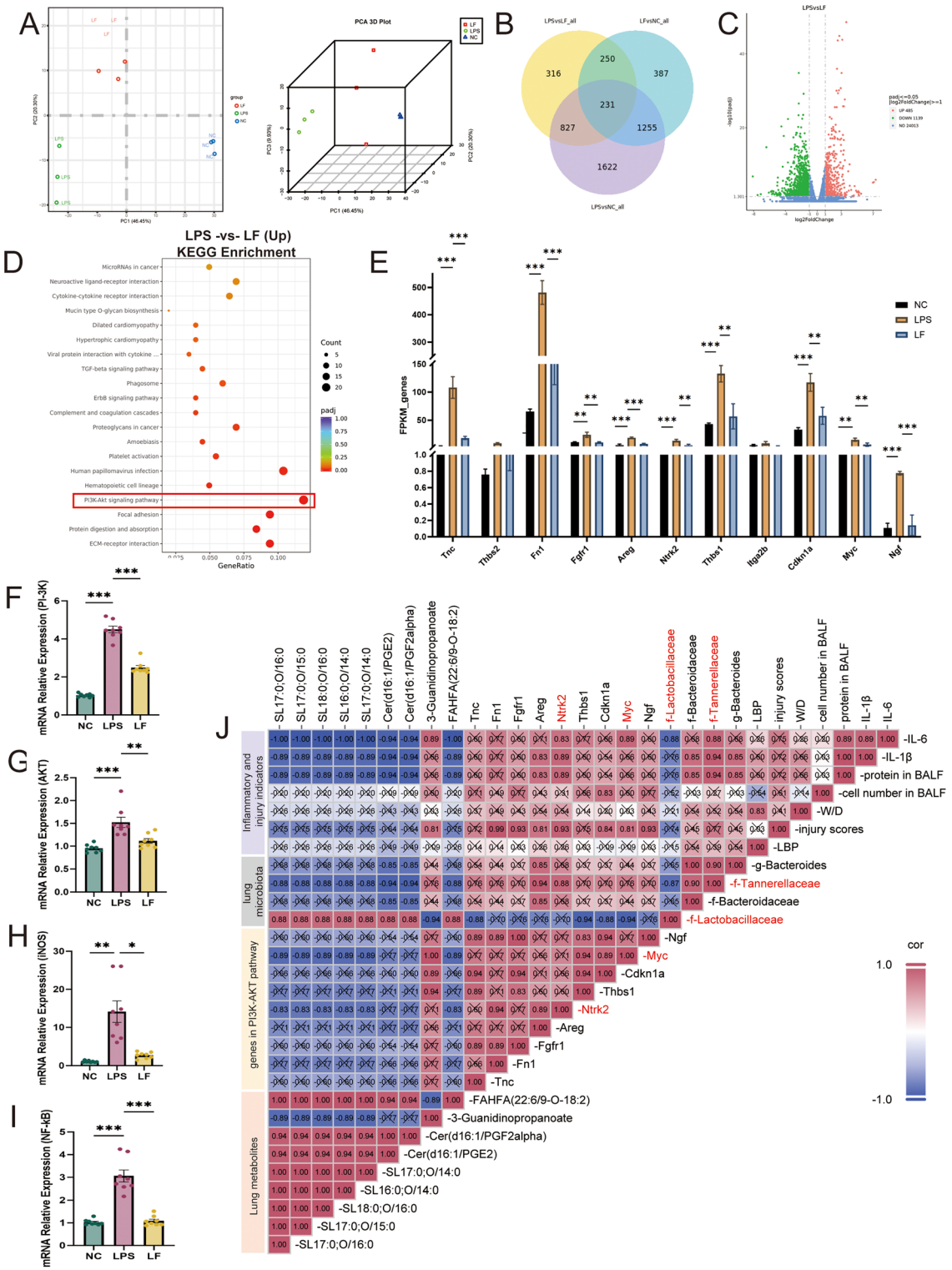

Fig. 5 (A) 2D and 3D principal component analysis (PCA) among the three groups. (B) Venn diagram of differential genes. (C) Volcano plot of differential genes. (D) Upregulated pathways in the LPS group of KEGG pathway enrichment analysis. (E) The FPKM of key genes through the PI3K–AKT signaling pathway. (F–I) The mRNA relative expression of PI3K, AKT, iNOS, and NF-κB. (J) Using Spearman's analysis, correlations were established between inflammatory indicators, injury indicators, pulmonary metabolites, genes of the PI3K–AKT pathway, and pulmonary microecology; the symbol "×" indicates that $p > 0.05$. Data are presented as the mean ± standard error of the mean (mean ± SEM); $^{*}p < 0.05$, $^{**}p < 0.01$ and $^{***}p < 0.001$.

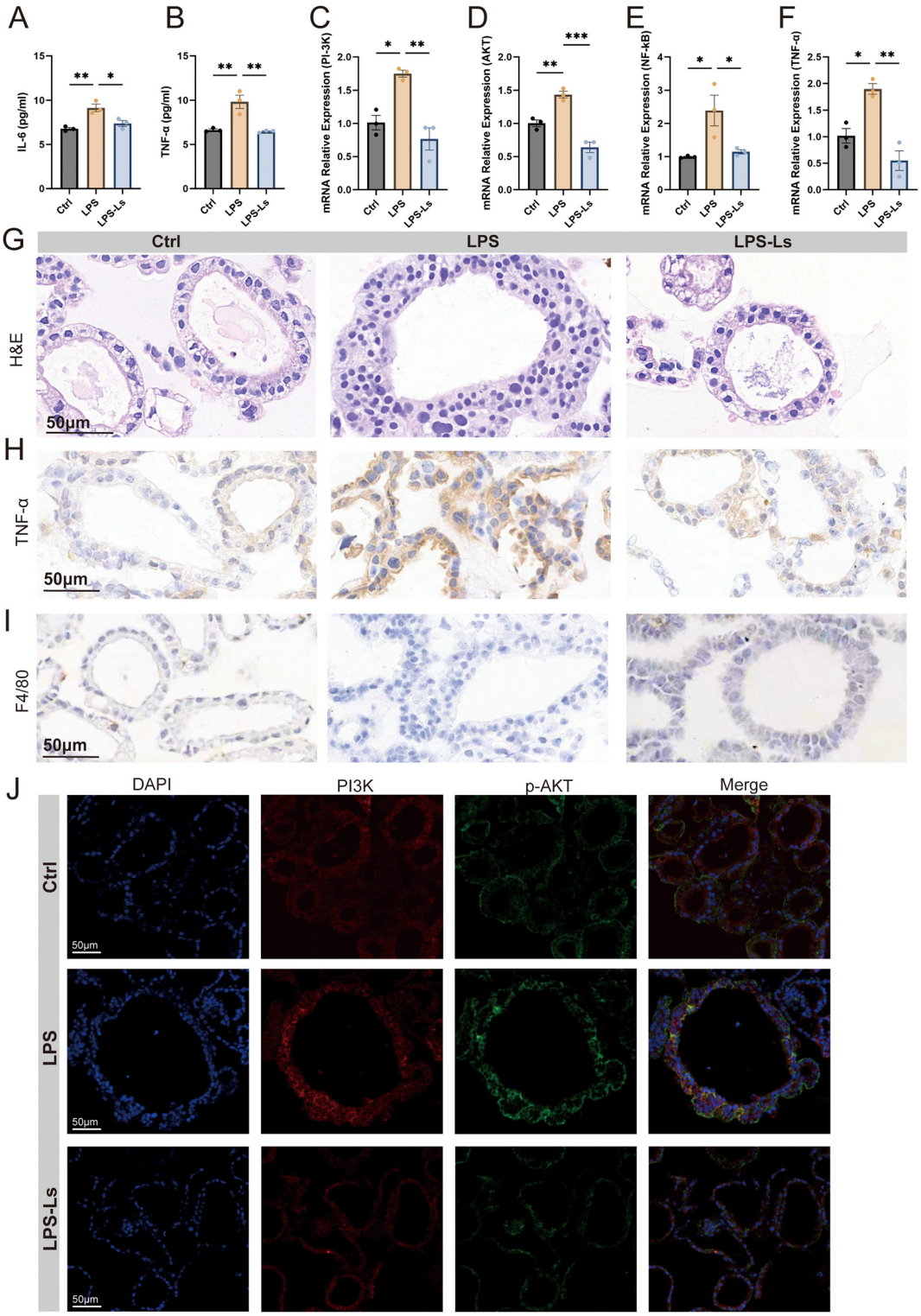

Fig. 6 (A and B) IL-6 and TNF-α level in the lung organoid culture supernatant. (C–F) The mRNA relative expression of PI3K, AKT, NF-κB and TNF-α in lung organoids. (G) H&E staining of lung organoids. (H) Immunohistochemical staining of TNF-α in lung organoids. (I) Immunohistochemical staining of F4/80 in lung organoids. (J) Immunofluorescence staining of PI3K and p-AKT in lung organoids – DAPI (blue), PI3K (red), and p-AKT (green). Data are presented as the mean ± standard error of the mean (mean ± SEM); *$p < 0.05$, **$p < 0.01$ and ***$p < 0.001$.

immunohistochemical staining revealed that the expression of TNF-α in alveolar organoids was significantly increased, suggesting a pronounced inflammatory response. The morphology of the organoids in the LPS-Ls group was significantly improved, and the cell degeneration, necrosis and inflammatory responses were also significantly alleviated. The expression of F4/80 in the LPS group was not significantly different from that in the LPS-LS group and Ctrl group (Fig. 6I), suggesting that there was no spontaneous differentiation of macrophages in pulmonary organoids. LPS could directly drive the alveolar epithelial cells to cause cell damage and an inflammatory response, and the CFS of *L. fermentum* could inhibit the inflammatory response of epithelial cells. As shown in Fig. 6J, the cytoplasm and cell membrane of the Ctrl group and LPS-Ls group showed weak green fluorescence, while the cell membrane and cell membrane of the LPS group showed diffuse enhanced green fluorescence, and the LPS group showed slightly stronger red fluorescence than the LPS-LS group. These results suggested that the CFS of *L. fermentum* could inhibit the excessive activation of the PI3K–AKT pathway in lung organoids induced by LPS.

Discussion

In this study, we identified a multi-layered protective mechanism by which *L. fermentum* attenuated acute lung injury through coordinated regulation of the gut–lung axis, pulmonary microecology, and epithelial inflammatory signaling. Firstly, ALI caused an acute inflammatory response, marked disruption of the integrity of the gut barrier and alterations in the gut microbiota, which were effectively restored by *L. fermentum*. Second, *L. fermentum* reengineered the lung microbiota; in particular, it increased the abundance of Lactobacillaceae, regulated lung transcription and metabolism, and ameliorated epithelial damage and inflammatory cell infiltration. Third, the CFS from *L. fermentum* was rich in microbial metabolites that directly protected alveolar organoids from LPS-induced injury by inhibiting PI3K–AKT activation. Taken together, these data provide a mechanistic framework linking microbial regulation, metabolism, and epithelial immunity in ALI.

ALI triggered a cycle of inflammation and microbial imbalance, which was characterized by elevated inflammatory mediators, damage to the alveolar epithelium, and increased protein-rich exudates.[28–30] The severe inflammatory response led to dysfunction of the intestinal barrier, allowing microorganisms and their metabolites to pass through the barrier and enter the lungs, thereby further activating the immune response in the distal lung mucosa.[2,31–39] The epithelial barrier, which is connected by a series of protein complexes such as tight junction proteins (ZO-1 and Claudin-1), is an important part of maintaining the stability of the gut–lung structure and immune homeostasis.[40] Consistent with this model, our findings revealed decreased expression of tight junction proteins and increased systemic inflammation following LPS challenge. Importantly, intragastric administration of *L. fermentum* restored the barrier protein levels and ameliorated circulating LBP, indicating that its primary mechanism of action involved the stabilization of mucosal integrity and the reduction of systemic leakage.

A noteworthy observation in this study was the increased abundance of Lactobacillaceae in the lung after *L. fermentum* intervention. Although the gut–lung microbial communication was well recognized, the direct regulation of lung microecology by gut probiotics remains unclear. Studies have confirmed that there is a significant correlation between the bacteria in the extraintestinal tissues regulated by gut-origin probiotics and the metabolic network.[41] In the LPS-induced sepsis model, *L. fermentum* pretreatment protected organ damage through antioxidant effects and reduction of pro-inflammatory factors such as TNF-α and IL-6.[42] Gut microbial products crossed the gut epithelial cells and affected distal organs directly or indirectly through the regulation of gut hormones.[43] Symbiotic bacteria can migrate to various tissues throughout the body in a stable state, but the specific mechanism remains unclear. Some studies suggested that a high bacterial load may facilitate the transfer of certain bacteria from the gut to the mesenteric lymph nodes, or through extracellular vesicles produced by dendritic cells to enter the circulation and be transported to distant organs.[41,44,45] Our findings suggest that microbial-derived metabolites or immunomodulatory signals may reach the lungs and reconfigure the local niche, thereby enhancing resistance to epithelial injury. This gut-derived modulation of the lung microbiota represents a novel aspect of gut–lung interactions and may partially explain the significant changes observed in the lung tissue.

The metabolites produced by the gut microbiota can be transmitted through the gut–lung axis to the lungs and participate in the pathogenesis of lung diseases.[46–48] Sphingolipids are structural components of membranes that regulate pulmonary mucosal immunity *via* endogenous lipids, while also exerting paracrine effects to defend against pathogens and alleviate inflammation.[39] In patients with pneumonia and in animal models of ALI induced by LPS, the levels of sphingosine were significantly disrupted, and the occurrence and development of ALI were significantly associated with the sphingolipid metabolic pathway.[49–51] Modulating sphingolipid metabolism has thus emerged as a promising therapeutic strategy, as evidenced by a rat ALI study in which the Tongfu Xingshen capsule alleviated gut barrier damage and improved lung injury by increasing the abundance of *Lactobacillus* and *Allobaculum*,[52] while concurrently reversing sphingolipid metabolic dysregulation. Eicosanoids are highly active lipid mediators produced by the oxidation of 20-carbon polyunsaturated fatty acids through cyclooxygenase, lipoxygenase and cytochrome P450 pathways.[53] They acted locally through G protein-coupled receptors or nuclear receptors, and were widely involved in inflammation, immune response and physiological and pathological processes of the gastrointestinal tract.[54] The levels of eicosanoids derived from arachidonic acid, such as PGD_2, PGE_2, TXA_2 and LTB_4, were elevated in the

inflamed gut mucosa, and these substances were correlated with disease activity or severity.[55–57] In addition, the metabolomic results revealed changes in triterpenoids and their derivatives. Triterpenoids and their derivatives have immunomodulatory activity and show neutrophil elastase inhibition.[58,59] *L. fermentum* intervention caused extensive reprogramming of gut and pulmonary metabolic networks.

The PI3K/AKT signaling pathway is a crucial intracellular communication hub that regulates essential biological processes, including metabolism and inflammatory responses.[60] A substantial body of evidence supports its pivotal role in the pathogenesis and treatment of ALI. For instance, Jingfang granules have been shown to alleviate pulmonary edema and inflammation in ALI mice by inhibiting the PI3K/Akt/mTOR axis and modulating associated carbon metabolism pathways.[61] In another study, acute ozone exposure induced bronchial epithelial damage and ferroptosis by activating TRPA1 *via* PI3K/AKT signaling, which subsequently disrupted mitochondrial function.[62] Furthermore, the pathway exhibited significant crosstalk with other metabolic processes; notably, sphingolipid metabolism was identified as strongly interrelated with the PI3K signaling pathway.[63] Both *in vivo* and *in vitro* studies further established PI3K/AKT as a central regulator of macrophage polarization—specifically balancing M1/M2a phenotypes—in the context of ALI intervention.[64] This was consistent with our findings. *L. fermentum* exhibited a dual protective role: the whole bacterium modulates systemic immunity to reduce the lung macrophage influx, while its CFS directly targets the alveolar epithelium to suppress PI3K–AKT-driven inflammatory signaling.

Crucially, the results of our *in vitro* studies using macrophageless alveolar organoids showed that LPS alone directly activated PI3K–AKT signaling within epithelial cells, suggesting that epithelial autoinflammation is a major driver of injury, independent of immune cell recruitment. For example, one study showed that some of the succinate found in the lungs came from the gut. It can aggravate ALI caused by intestinal ischemia–reperfusion injury by promoting macrophage polarization and the PI3K/AKT/HIF-1α signaling pathway.[65] Treatment with CFS effectively inhibited PI3K–AKT activation and reduced the secretion of inflammatory mediators, confirming that probiotic-derived metabolites could directly act on epithelial cells. When combined with *in vivo* findings, these observations support a unifying model in which *L. fermentum* reduces systemic inflammatory inputs from the gut, remodels the lung microecology, and directly modulates intraepithelial signaling that collectively contribute to the mitigation of lung injury.

Several limitations remain in this study. First, the precise mechanism by which *L. fermentum* translocates from the intestinal tract to the lungs following oral gavage remains to be fully delineated. Second, while pulmonary metabolomic analysis indicated significant alterations in sphingolipid metabolism upon *L. fermentum* intervention, the specific metabolites responsible for these changes could not be conclusively identified. Furthermore, due to the acidic growth conditions required for *L. fermentum*, direct co-culture with alveolar organoids was not feasible, preventing direct observation of their interaction. Although similar validation results were obtained using low concentrations of CFS as a surrogate for *L. fermentum*, the full effect of *L. fermentum* may be underestimated.

L. fermentum can not only regulate the systemic immunity and improve the infiltration of macrophages and neutrophils, but also inhibit the autoinflammatory response of alveolar epithelial cells. In addition, *L. fermentum* can reshape the lung microecology, affect sphingolipid metabolism, and inhibit the PI3K–AKT signaling pathway, thereby reducing lung injury. These findings not only deepen our understanding of the mechanistic basis of probiotic-mediated protection against ALI, but also provide strong preclinical evidence for the development of *L. fermentum* as a potential adjuvant therapeutic agent. In future studies, we should focus on identifying the specific active metabolites responsible for their beneficial effects and explore their therapeutic potential in patients with acute lung injury due to clinical infection or sepsis.

Methods

Strain and culture conditions

L. fermentum (CECT5716) was anaerobically cultured in de Man–Rogosa–Sharpe (MRS) broth at 37 °C for 24 hours. *L. fermentum* was then collected by centrifugation at 4000*g* for 10 min at 4 °C, washed twice with PBS, and finally resuspended in PBS to a concentration of 3×10^9 CFU mL^{-1}. Fresh suspensions of *L. fermentum* were prepared daily for mouse gavage.

After centrifugation under the same conditions, the supernatant was collected and filtered through a 0.22-micron membrane to remove free bacteria, resulting in a cell-free supernatant (CFS). The pH value of the CFS was adjusted for use in subsequent experiments.

Animal experiments

Male C57BL/6 mice (6–8 weeks old, 22 ± 0.5 g) were housed under specific pathogen-free conditions with a 12 h/12 h light/dark cycle, stable temperature and humidity. After acclimation, the mice were randomly divided into three groups (Fig. 1A, all groups n = 8: NC group, LPS group, and LF group). The LF group received a daily oral gavage of *L. fermentum* for 21 days, while the NC and LPS groups were administered PBS as a vehicle control. On day 22, acute lung injury was induced in the LPS and LF groups *via* intratracheal instillation of LPS (5 mg kg^{-1}; Sigma-Aldrich, UK), with the NC group receiving an equal volume of sterile saline. All animals were euthanized by a sodium pentobarbital injection five days after modeling.

Serum parameter assay analysis

Serum was separated from blood samples by centrifugation at 3000*g* for 15 min at 4 °C and stored at −80 °C until analysis. Inflammatory cytokine levels were assayed using a mouse cyto-

kine 23-plex kit (Bio-Rad, USA), and the LPS binding protein (LBP) concentrations were determined by using an ELISA kit (Abcam, ab269542). All procedures were conducted in accordance with the manufacturers' instructions, with $n = 8$ replicates per group.

Bronchoalveolar lavage fluid (BALF) assay analysis

BALF was collected *via* endotracheal lavage with PBS following euthanasia. After centrifugation (800*g*, 4 °C, 10 min), supernatants were aliquoted and stored at −80 °C. Cell pellets were treated with RBC lysis buffer (5–10 min) and resuspended for counting using a Countess automated cell counter (Thermo Fisher Scientific). The total protein content was quantified using a Pierce™ BCA assay. Levels of cytokines (IL-1β and IL-6) and lactate dehydrogenase (LDH) activity were measured using the respective ELISA kits (Abcam, Cambridge, UK) according to the manufacturer's instructions. For all groups $n = 8$.

Lung tissue W/D ratio

The right middle lung lobe was harvested on day 26, and the wet weight (W) was measured immediately after gently wiping blood from the surface. All right middle lobe tissues were then placed in an oven at 70 °C for continuous drying for 72 hours, and then the dry weight (D) was measured. The severity of pulmonary tissue edema was evaluated by calculating the W/D ratio. For all groups $n = 8$.

Histopathological analysis

The lung and colon tissue samples were fixed with the SIF formalin fixative for 24 hours. Then, the tissues of the lungs and colon were embedded in paraffin and cut into 2 μm sections. The lung tissue was stained with hematoxylin and eosin (H&E) to observe the tissue morphology. Lung tissues were immunostained for the anti-F4/80 antibody and the anti-myeloperoxidase (MPO) antibody. Colon samples were immunostained for the anti-zonula occludens-1 (ZO-1) antibody, the anti-Occludin antibody and the anti-mucin-2 (MUC-2) antibody to evaluate gut barrier integrity. Pathological scores of lung tissues were assigned independently by two certified pathologists using a double-blind protocol. The images were scanned using a Pannoramic MIDI scanner (3DHISTECH, Budapest, Hungary). For all groups $n = 3$.

Real-time fluorescence quantitative PCR analysis

The RNA was extracted from the lungs and colon, using the RNeasy Plus Mini kit (Qiagen, CA, USA). The obtained RNA was then reverse transcribed into complementary DNA (cDNA), using the PrimeScript™ RT kit (Takara, Kusatsu, Japan). Subsequently, the levels of expression of target genes were measured using the ViiA7 real-time PCR system (Applied Biosystems, Waltham, Massachusetts, USA) based on the $2^{-\Delta\Delta CT}$ method (with GAPDH as a control) using the SYBR Premix Ex Taq II reagent (Takara). The primer sequences of the genes used for RT-qPCR analysis are shown in SI Table S1. For all groups $n = 8$.

16S rRNA sequencing

Total genomic DNA was extracted from the lung and stool samples using the FastPure Stool DNA Isolation Kit (MJYH) following the manufacturer's protocol. PCR amplification of the V3–V4 variable regions was performed with the use of universal primer sequences (forward sequence: CCTAYGGGRBGCASCAG, reverse sequence: GGACTACNNGGGTATCTAAT). After identification, the data were sequenced on an Illumina NovaSeq6000 platform (Illumina Inc., CA, USA) and the libraries were constructed. The data were imported into QIIME2 for processing. By using the DADA2 plugin, the data were then clustered into amplicon sequence variant (ASV) groups and classified according to the Silva 138 database in QIIME2. α- and β-Diversity analyses were performed in QIIME2. Differential taxa between groups were identified using LEfSe analysis (LDA, $p < 0.05$). For all groups $n = 8$.

Transcriptome analysis

Lung tissue RNA was extracted, and a library was constructed and sequenced as described previously.[66] Differential transcript analysis among the three groups was later performed using the R package DESeq2, and the p values obtained were adjusted to control for error incidence by using Benjamini and Hochberg's approach. Genes with $P_{adj} < 0.05$ by DESeq2 were considered as having differential transcripts. For all groups $n = 3$.

Non-targeted metabolomic analysis of the lung tissue

Lung tissue samples and feces samples ($n = 6$ per group) were homogenized in 400 μL methanol : water (4 : 1) using a cryogenic tissue grinder (6 min, −10 °C, 50 Hz), followed by low-temperature ultrasonic extraction (30 min, 5 °C, 40 kHz). After incubation at −20 °C for 30 min, samples were centrifuged (13 000*g*, 4 °C, 15 min) and supernatants were collected for LC-MS analysis. Metabolite profiling was performed using an Orbitrap Q Exactive™ HF mass spectrometer (Thermo Fisher Scientific). Raw data were processed using Progenesis QI v3.0 (Waters) for peak identification, alignment, and correction, generating a data matrix containing m/z and intensity values. Metabolites were annotated against the KEGG and HMDB databases. Differential metabolites were identified with thresholds of $p < 0.05$, VIP > 1, and FC < 1.

Lung organoids

After cleaning the mouse lung tissue with PBS, it was minced and digested until the tissue became loose. After terminating the digestion, the sample was centrifuged at 1500 rpm for 3 minutes, the supernatant was discarded, and a balanced salt solution was added for resuspension. Then, the cells were filtered through a 100 μm cell sieve, followed by another 1500 rpm centrifugation process for 3 minutes and the supernatant was discarded. The cell precipitate was resuspended in a complete medium for lung organoid expansion (RISEZI Biotechnology Co, Ltd, RSQ-OCM1109) and prepared into a cell suspension of 1–20 × 10^5 mL^{-1}. The cell suspension was inoculated into the matrix gel (Corning, 356231) and cultured

in a CO_2 incubator (37 °C, 5% CO_2 concentration).[67] The mature pulmonary organoids were randomly grouped, namely the Ctrl group, the LPS group, and the LPS-Ls group (for all groups n = 3). To the LPS group was added 50 μg mL^{-1} LPS and it was treated for 48 hours. The LPS-Ls group was pre-treated with 30% CFS for 24 hours before adding LPS for 48 hours. Samples were collected after 48 hours, and some were fixed with paraformaldehyde for subsequent pathological experiments. The others were extracted for RNA for subsequent experiments. The supernatant of organoids was stored at −80 °C.

A portion of the organoids was fixed in 4% paraformaldehyde, embedded in paraffin, and sectioned for histological analysis. The lung alveolar organoids were identified using an anti-RAGE antibody and an anti-prosurfactant protein C antibody. Sections were stained with H&E for general morphological assessment. Immunostaining for TNF-α was performed to evaluate lung organoid damage. Immunofluorescence experiments were performed on organoids using the PI3K/AKT signalling pathway panel (contains AKT1 + AKT2 + AKT3 (phospho S472 + S473 + S474) and PI 3 kinase p85 alpha). The images were scanning using a Pannoramic MIDI scanner (3DHISTECH, Budapest, Hungary). For all groups n = 3.

Statistical analysis

All statistical analyses were performed using IBM SPSS Statistics 22.0 and GraphPad Prism 10.1. Continuous variables with normal distribution are presented as mean ± SD, and those with non-normal distribution are expressed as median (IQR). The Shapiro–Wilk test was applied to assess data normality. For comparisons between two groups, a two-tailed Student's *t*-test or Mann–Whitney *U* test was used as appropriate. Ordinary analysis of variance (ANOVA) was used for comparisons among more than two groups with equal standard deviations, otherwise, Brown–Forsythe and Welch ANOVA were performed. Pairwise comparisons were conducted using Tukey's *post hoc* test. Figures were generated using GraphPad Prism 10.0 and R (version 4.2). Significance levels are denoted as $*p < 0.05$, $**p < 0.01$ and $***p < 0.001$.

Author contributions

JLN, YFC, and LJL contributed to the design of this study. JLN and JS conducted the main experiments and data analysis. JLN, JS, FJW, YCW, BQ, ZYZ, QHX, SJL, QQX, TLS and YXZ participated in the animal experiments and data collection. JLN wrote the manuscript. YFC and LJL revised the manuscript. All authors read and approved the final manuscript.

Conflicts of interest

There are no conflicts to declare.

Ethics statement

All animal procedures were performed in accordance with the Guidelines for Care and Use of Laboratory Animals of Zhejiang University, and approved by the Animal Ethics Committee of Animal Experiments (Zhejiang, China) of the First Affiliated Hospital of Zhejiang University (approval no. 2023-969).

Data availability

Data for this article, including feces and lung 16S rRNA data, are available at the National Center for Biotechnology Information (https://www.ncbi.nlm.nih.gov/sra/PRJNA1345011).

Supplementary information (SI) is available. The supplementary file includes primer sequences, antibody information, and information on metabolites. See DOI: https://doi.org/10.1039/d5fo04619j.

Acknowledgements

We thank BioRender (https://app.biorender.com) for the graphical abstract drawings.

This work was supported by the National Key R&D Program of China (2022YFC3602000), the Natural Science Foundation of China (32270068), the Fundamental Research Funds for the Central Universities (2025ZFJH03), the Central Guidance Fund for Local Science and Technology Development (2024ZY01054), the Shandong Provincial Laboratory Project (SYS202202) and the Research Project of Jinan Microecological Biomedicine Shandong Laboratory (JNL-2022001A).

References

1 J. Tang, L. Xu, Y. Zeng, *et al.*, Effect of gut microbiota on LPS-induced acute lung injury by regulating the TLR4/NF-kB signaling pathway, *Int. Immunopharmacol.*, 2021, **91**, 107272.
2 X. Zhou and Y. Liao, Gut–lung crosstalk in sepsis-induced acute lung injury, *Front. Microbiol.*, 2021, **12**, 779620.
3 K. Komiya, T. Akaba, Y. Kozaki, *et al.*, A systematic review of diagnostic methods to differentiate acute lung injury/acute respiratory distress syndrome from cardiogenic pulmonary edema, *Crit. Care*, 2017, **21**(1), 228.
4 S. R. Lewis, M. W. Pritchard, C. M. Thomas, *et al.*, Pharmacological agents for adults with acute respiratory distress syndrome, *Cochrane Database Syst. Rev.*, 2019, **7**(7), Cd004477.
5 C. Chen, J. Lin, X. Wang, *et al.*, Novel insights into immune mechanisms in acute lung injury: Focusing on gut microbiota and its metabolites, *Microbiol. Res.*, 2025, **300**, 128279.
6 C. B. Hildebrand, R. Lichatz, A. Pich, *et al.*, Short-chain fatty acids improve inflamm-aging and acute lung injury in old mice, *Am. J. Physiol. Lung Cell. Mol. Physiol.*, 2023, **324**(4), L480–Ll92.

7 X. Hu, Z. Han, R. Zhou, *et al.*, Altered gut microbiota in the early stage of acute pancreatitis were related to the occurrence of acute respiratory distress syndrome, *Front. Cell. Infect. Microbiol.*, 2023, **13**, 1127369.
8 T. P. Wypych, L. C. Wickramasinghe and B. J. Marsland, The influence of the microbiome on respiratory health, *Nat. Immunol.*, 2019, **20**(10), 1279–1290.
9 X. Yi, J. Gao and Z. Wang, The human lung microbiome-A hidden link between microbes and human health and diseases, *iMeta*, 2022, **1**(3), e33.
10 P. Liang, Y.-H. Niu, S.-Y. Zhu, *et al.*, The role of lung microbiome in lung cancer: from mechanisms to clinical implications, *Infect. Microbes Dis.*, 2025, **7**(4), 209–216.
11 L. Tang, S. Gu, Y. Gong, *et al.*, Clinical significance of the correlation between changes in the major intestinal bacteria species and COVID-19 severity, *Engineering*, 2020, **6**(10), 1178–1184.
12 K. Bao, M. Wang, L. Liu, *et al.*, Jinhong decoction protects sepsis-associated acute lung injury by reducing intestinal bacterial translocation and improving gut microbial homeostasis, *Front. Pharmacol.*, 2023, **14**, 1079482.
13 Q. Le Bastard, T. Ward, D. Sidiropoulos, *et al.*, Fecal microbiota transplantation reverses antibiotic and chemotherapy-induced gut dysbiosis in mice, *Sci. Rep.*, 2018, **8**(1), 6219.
14 F. Hua, E. Cui, L. Lv, *et al.*, Fecal microbiota transplantation from HUC-MSC-treated mice alleviates acute lung injury in mice through anti-inflammation and gut microbiota modulation, *Front. Microbiol.*, 2023, **14**, 1243102.
15 J. Shen, S. Wang, H. Xia, *et al.*, Akkermansia muciniphila attenuated lipopolysaccharide-induced acute lung injury by modulating the gut microbiota and SCFAs in mice, *Food Funct.*, 2023, **14**(23), 10401–10417.
16 P. Gutiérrez-Castrellón, T. Gandara-Martí, Y. A. A. T. Abreu, *et al.*, Probiotic improves symptomatic and viral clearance in Covid19 outpatients: A randomized, quadruple-blinded, placebo-controlled trial, *Gut Microbes*, 2022, **14**(1), 2018899.
17 N. P. West, D. B. Pyne, A. W. Cripps, *et al.*, *Lactobacillus fermentum* (PCC®) supplementation and gastrointestinal and respiratory-tract illness symptoms: A randomised control trial in athletes, *Nutr. J.*, 2011, **10**, 30.
18 V. Prakash, A. Madhavan, A. P. Veedu, *et al.*, Harnessing the probiotic properties and immunomodulatory effects of fermented food-derived *Limosilactobacillus fermentum* strains: Implications for environmental enteropathy, *Front. Nutr.*, 2023, **10**, 1200926.
19 C. L. Ramos, L. Thorsen, R. F. Schwan, *et al.*, Strain-specific probiotics properties of *Lactobacillus fermentum*, *Lactobacillus plantarum* and *Lactobacillus brevis* isolates from Brazilian food products, *Food Microbiol.*, 2013, **36**(1), 22–29.
20 K. Naghmouchi, Y. Belguesmia, F. Bendali, *et al.*, *Lactobacillus fermentum*: A bacterial species with potential for food preservation and biomedical applications, *Crit. Rev. Food Sci. Nutr.*, 2020, **60**(20), 3387–3399.
21 Y. Liu, Z. Lin, M. Yang, *et al.*, *Lactiplantibacillus plantarum* HCS03-001 and *Lacticaseibacillus paracasei* HCS17-040 synergize to combat *Helicobacter pylori* colonization and gastric inflammation, *Infect. Microbes Dis.*, 2025, **7**(3), 135–147.
22 Q. Chen, M. Liu, Y. Lin, *et al.*, Topography of respiratory tract and gut microbiota in mice with influenza A virus infection, *Front. Microbiol.*, 2023, **14**, 1129690.
23 J. C. Valdéz, M. C. Peral, M. Rachid, *et al.*, Interference of *Lactobacillus plantarum* with *Pseudomonas aeruginosa* in vitro and in infected burns: The potential use of probiotics in wound treatment, *Clin. Microbiol. Infect.*, 2005, **11**(6), 472–479.
24 S. De Marco, M. Sichetti, D. Muradyan, *et al.*, Probiotic cell-free supernatants exhibited anti-inflammatory and antioxidant activity on human gut epithelial cells and macrophages stimulated with LPS, *Evid. Based Complement. Alternat. Med.*, 2018, **2018**, 1756308.
25 S. Chandla, K. Harjai and G. Shukla, Combinatorial therapeutic strategy of biogenics derived from *Lactobacillus fermentum* PUM and zingerone against *Pseudomonas aeruginosa* PAO1-induced surgical site infection: An experimental study, *Probiotics Antimicrob. Proteins*, 2022, **14**(4), 712–726.
26 R. Kumar, A. Sharma, M. Gupta, *et al.*, Cell-free culture supernatant of probiotic *Lactobacillus fermentum* protects against H(2)O(2)-induced premature senescence by suppressing ROS-Akt-mTOR axis in murine preadipocytes, *Probiotics Antimicrob. Proteins*, 2020, **12**(2), 563–576.
27 A. Shieh, M. Epeldegui, A. S. Karlamangla, *et al.*, Gut permeability, inflammation, and bone density across the menopause transition, *JCI Insight*, 2020, **5**(2), e134092.
28 X. Li, M. Jamal, P. Guo, *et al.*, Irisin alleviates pulmonary epithelial barrier dysfunction in sepsis-induced acute lung injury via activation of AMPK/SIRT1 pathways, *Biomed. Pharmacother.*, 2019, **118**, 109363.
29 R. P. Dickson, J. R. Erb-Downward and G. B. Huffnagle, Homeostasis and its disruption in the lung microbiome, *Am. J. Physiol.: Lung Cell. Mol. Physiol.*, 2015, **309**(10), L1047–L1055.
30 R. P. Dickson, J. R. Erb-Downward and G. B. Huffnagle, Towards an ecology of the lung: New conceptual models of pulmonary microbiology and pneumonia pathogenesis, *Lancet Respir. Med.*, 2014, **2**(3), 238–246.
31 J. Wang, X. Xue, X. Zhao, *et al.*, Forsythiaside A alleviates acute lung injury by inhibiting inflammation and epithelial barrier damages in lung and colon through PPAR-γ/RXR-α complex, *J. Adv. Res.*, 2024, **60**, 183–200.
32 J. A. Clark and C. M. Coopersmith, Intestinal crosstalk: A new paradigm for understanding the gut as the "motor" of critical illness, *Shock*, 2007, **28**(4), 384–393.
33 T. B. Clarke, K. M. Davis, E. S. Lysenko, *et al.*, Recognition of peptidoglycan from the microbiota by Nod1 enhances systemic innate immunity, *Nat. Med.*, 2010, **16**(2), 228–231.
34 Y. Lu, Y. Wu, M. Huang, *et al.*, Fuzhengjiedu formula exerts protective effect against LPS-induced acute lung injury via gut-lung axis, *Phytomedicine*, 2024, **123**, 155190.

35 Z. M. Zhang, Y. C. Wang, L. Chen, *et al.*, Protective effects of the suppressed NF-κB/TLR4 signaling pathway on oxidative stress of lung tissue in rat with acute lung injury, *Kaohsiung J. Med. Sci.*, 2019, **35**(5), 265–276.
36 L. Wang, Y. Cai, J. Garssen, *et al.*, The bidirectional gut–lung axis in chronic obstructive pulmonary disease, *Am. J. Respir. Crit. Care Med.*, 2023, **207**(9), 1145–1160.
37 Y. Wang, Y. Wang, J. Ma, *et al.*, YuPingFengSan ameliorates LPS-induced acute lung injury and gut barrier dysfunction in mice, *J. Ethnopharmacol.*, 2023, **312**, 116452.
38 M. Jeyanathan, M. Vaseghi-Shanjani, S Afkhami, *et al.*, Parenteral BCG vaccine induces lung-resident memory macrophages and trained immunity via the gut-lung axis, *Nat. Immunol.*, 2022, **23**(12), 1687–1702.
39 M. Candelli, L. Franza, G. Pignataro, *et al.*, Interaction between lipopolysaccharide and gut microbiota in inflammatory bowel diseases, *Int. J. Mol. Sci.*, 2021, **22**(12), 6242.
40 C. A. Akdis, Does the epithelial barrier hypothesis explain the increase in allergy, autoimmunity and other chronic conditions?, *Nat. Rev. Immunol.*, 2021, **21**(11), 739–751.
41 Z. Zhu, J. Cai, W. Hou, *et al.*, Microbiome and spatially resolved metabolomics analysis reveal the anticancer role of gut *Akkermansia muciniphila* by crosstalk with intratumoral microbiota and reprogramming tumoral metabolism in mice, *Gut Microbes*, 2023, **15**(1), 2166700.
42 B. Arribas, M. E. Rodríguez-Cabezas, M. Comalada, *et al.*, Evaluation of the preventative effects exerted by *Lactobacillus fermentum* in an experimental model of septic shock induced in mice, *Br. J. Nutr.*, 2009, **101**(1), 51–58.
43 V. Bozzetti and S. Senger, Organoid technologies for the study of intestinal microbiota–host interactions, *Trends Mol. Med.*, 2022, **28**(4), 290–303.
44 M. Muraca, L. Putignani, A. Fierabracci, *et al.*, Gut microbiota-derived outer membrane vesicles: Under-recognized major players in health and disease?, *Discovery medicine*, 2015, **19**(106), 343–348.
45 A. C. McPherson, S. P. Pandey, M. J. Bender, *et al.*, Systemic immunoregulatory consequences of gut commensal translocation, *Trends Immunol.*, 2021, **42**(2), 137–150.
46 N. Arpaia, C. Campbell, X. Fan, *et al.*, Metabolites produced by commensal bacteria promote peripheral regulatory T-cell generation, *Nature*, 2013, **504**(7480), 451–455.
47 R. Kapur, M. Kim, J. Rebetz, *et al.*, Gastrointestinal microbiota contributes to the development of murine transfusion-related acute lung injury, *Blood Adv.*, 2018, **2**(13), 1651–1663.
48 T. J. Schuijt, J. M. Lankelma, B. P. Scicluna, *et al.*, The gut microbiota plays a protective role in the host defence against pneumococcal pneumonia, *Gut*, 2016, **65**(4), 575–583.
49 Y. Chen, M. Peng, W. Li, *et al.*, Inhibition of inflammasome activation via sphingolipid pathway in acute lung injury by Huanglian Jiedu decoction: An integrative pharmacology approach, *Phytomedicine*, 2022, **107**, 154469.
50 H. Grassmé, B. Henry, R. Ziobro, *et al.*, β1-Integrin accumulates in cystic fibrosis luminal airway epithelial membranes and decreases sphingosine, promoting bacterial infections, *Cell Host Microbe*, 2017, **21**(6), 707–718.e8.
51 R. T. Okuro, M. N. Machado, N. V. Casquilho, *et al.*, The role of sphingolipid metabolism disruption on lipopolysaccharide-induced lung injury in mice, *Pulm. Pharmacol. Ther.*, 2018, **50**, 100–110.
52 R. Wang, C. Gan, B. Gong, *et al.*, Tongfu Xingshen capsule alleviates stroke-associated pneumonia-induced multiple organ injuries by modulating the gut microbiota and sphingolipid metabolism, *Phytomedicine*, 2025, **142**, 156756.
53 W. W. Christie and J. L. Harwood, Oxidation of polyunsaturated fatty acids to produce lipid mediators, *Essays Biochem.*, 2020, **64**(3), 401–421.
54 P. C. Calder, Eicosanoids, *Essays Biochem.*, 2020, **64**(3), 423–441.
55 K. Takeuchi and K. Amagase, Roles of cyclooxygenase, prostaglandin E2 and EP receptors in mucosal protection and ulcer healing in the gastrointestinal tract, *Curr. Pharm. Des.*, 2018, **24**(18), 2002–2011.
56 P. Sharon and W. F. Stenson, Enhanced synthesis of leukotriene B4 by colonic mucosa in inflammatory bowel disease, *Gastroenterology*, 1984, **86**(3), 453–460.
57 M. Masoodi, D. S. Pearl, M. Eiden, *et al.*, Altered colonic mucosal polyunsaturated fatty acid (PUFA) derived lipid mediators in ulcerative colitis: New insight into relationship with disease activity and pathophysiology, *PLoS One*, 2013, **8**(10), e76532.
58 R. A. Hill and J. D. Connolly, Triterpenoids, *Nat. Prod. Rep.*, 2020, **37**(7), 962–998.
59 G. Zheng, Y. Zhao, Z. Li, *et al.*, GLSP and GLSP-derived triterpenes attenuate atherosclerosis and aortic calcification by stimulating ABCA1/G1-mediated macrophage cholesterol efflux and inactivating RUNX2-mediated VSMC osteogenesis, *Theranostics*, 2023, **13**(4), 1325–1341.
60 I. Hers, E. E. Vincent and J. M. Tavaré, Akt signalling in health and disease, *Cell. Signalling*, 2011, **23**(10), 1515–1527.
61 X. Sun, H. Xiang, Z. Liu, *et al.*, Jingfang Granules () alleviates bleomycin-induced acute lung injury through regulating PI3K/Akt/mTOR signaling pathway, *J. Ethnopharmacol.*, 2024, **318**(Pt A), 116946.
62 J. Weng, Q. Liu, C. Li, *et al.*, TRPA1-PI3K/Akt-OPA1-ferroptosis axis in ozone-induced bronchial epithelial cell and lung injury, *Sci. Total Environ.*, 2024, **918**, 170668.
63 T. Wang, X. Li, G. Liao, *et al.*, AFB1 triggers lipid metabolism disorders through the PI3K/Akt pathway and mediates apoptosis leading to hepatotoxicity, *Foods*, 2024, **13**(1), 163.
64 X. Qiao, H. Wang, Y. He, *et al.*, Grape seed proanthocyanidin ameliorates LPS-induced acute lung injury by modulating M2a macrophage polarization via the TREM2/PI3K/Akt pathway, *Inflammation*, 2023, **46**(6), 2147–2164.
65 Y. H. Wang, Z. Z. Yan, S. D. Luo, *et al.*, Gut microbiota-derived succinate aggravates acute lung injury after intesti-

nal ischaemia/reperfusion in mice, *Eur. Respir. J.*, 2023, **61**(2), 2200840.

66 L. Lv, C. Yao, R. Yan, *et al.*, *Lactobacillus acidophilus* LA14 alleviates liver injury, *mSystems*, 2021, **6**(3), e0038421.

67 J. Zhu, J. Zhou, B. Feng, *et al.*, MSCs alleviate LPS-induced acute lung injury by inhibiting the proinflammatory function of macrophages in mouse lung organoid-macrophage model, *Cell. Mol. Life Sci.*, 2024, **81**(1), 124.